

Worcester Polytechnic Institute

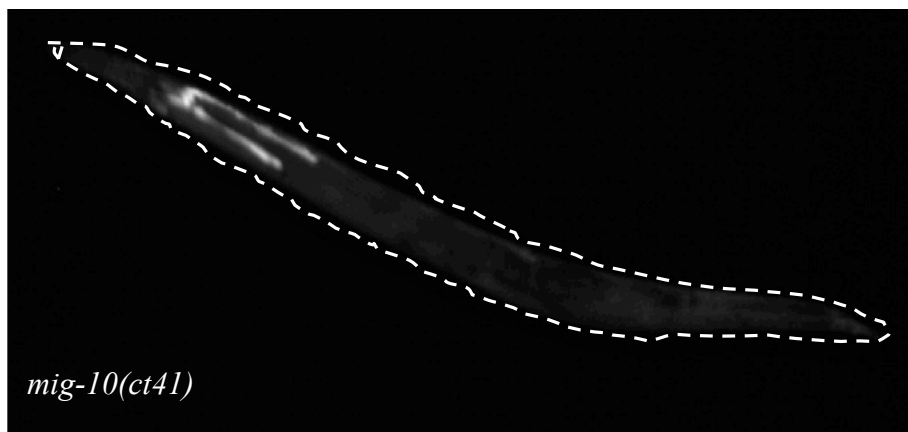
Abi-1 Interacts with Mig-10

Protein interaction in neuronal migration in
Caenorhabditis elegans

A Major Qualifying Project by:

Michelle Dubuke and Christina Grant

April 30th, 2009



Abstract

The process of neuronal migration is of great interest for neuron regeneration. MIG-10, a *C.elegans* homologue to vertebrate Lamellipodin (Lpd) and an Lpd-related molecule RIAM, is known to stimulate lamellipodia formation in directed neuronal migration, as well as cause truncation of the excretory canal. MIG-10, through Yeast Two Hybrid, was found to physically interact with Ablason Interacting Protein 1 (ABI-1) in vitro; those results are being verified using Co-IP in insect cells, and the in vivo interaction of the proteins was studied using RNAi expression knockdown. MIG-10 mutants (RY108), with a GFP-labeled excretory canal, had significantly increased truncation of the excretory canal when fed on ABI-1 RNAi. We concluded that MIG-10 and ABI-1 may reside in different pathways, but have overlapping functions.

Acknowledgements

Thanks to the Stringham lab for helpful discussion on results, as well as help with techniques and providing strains for the RNAi work.

Thanks to the Duffy lab for help with the CoIP experiments, for providing reagents and guidance.

We would like to thank Professor Sam Politz for discussion in the early phases of experimentation when we were trying to work out the problems with the RNAi system.

And finally, we would like to thank our advisor, Elizabeth Ryder, for all the help and guidance she gave us on this project. Without her, this would never have gotten off the ground.

Table of Contents

Abstract	2
Acknowledgements	3
Table of Contents	4
Table of Figures	6
Table of Tables	7
Introduction	8
Caenorhabditis elegans: Model Organism.....	10
MIG-10	10
Guidance cues and the function of Mig-10.....	12
MIG-10 in complex with other proteins	13
ABI-1	14
Project goals: Testing ABI-1’s interaction with MIG-10	15
Biochemical Analysis of the MIG-10/ABI-1 Interaction	16
<i>Yeast Two Hybrid System</i>	16
<i>Co-immunoprecipitation</i>	17
Project Goal: Testing MIG-10’s Physical Interaction with Other Proteins.....	18
Methods	19
RNAi Feeding Protocol	19
<i>Preparation of RNAi Plates</i>	19
<i>Inoculation and Seeding of RNAi bacterial strains</i>	19
<i>Transfer of worms to RNAi plates</i>	20
<i>Preparing slides for scoring of F1s and F2s from RNAi feeding</i>	21
<i>Quantification/Scoring of F1s and F2s from RNAi feeding</i>	22
<i>Statistical Analysis of Different Generations</i>	23
<i>Statistical Analysis of Different Strains</i>	24
PCR for generating Att Sites	25
BP recombination reaction	27
Transformation of competent cells	28
Isolation of plasmid DNA.....	28
Results	30
<i>abi-1</i> has a small, but very significant effect on excretory canal outgrowth	32
<i>abi-1</i> and <i>mig-10</i> show a genetic interaction	34
<i>unc-53</i> shows a borderline genetic interaction with <i>mig-10</i>	35
Controls used to show genetic interactions between proteins	36
Preparation of vectors for Co-immunoprecipitation experiments	37
<i>Generation of an Expression Vector</i>	38
PCR-based Generation of AttB Flanked Genes	38
Generation of Entry Vectors.....	39
Discussion	41
References	46
Appendices	48
Appendix A: RNAi Method Diagram.....	48
Appendix B: Chi-Square Tests, Data Combination.....	49

Appendix C: Chi-Square Test, Strain Comparisons52

Table of Figures

Figure 1 - Axonal Growth Cone with labeled lamellapodium and filopodia	9
Figure 2 - Schematic of regions of worms for quantification of truncation	23
Figure 3 - Sample table for data consolidation	23
Figure 4 - Sample table for chi-square analysis for strain comparison.....	24
Figure 5 - Comparison of Excretory Canal Truncation in <i>C. elegans</i> with RNAi.....	32
Figure 6 - Wildtype and <i>abi-1(tm494)</i> mutant.....	30
Figure 7 - <i>abi-1(tm494);abi-1(RNAi)</i>	31
Figure 8 - <i>mig-10(ct41)</i> and <i>mig-10(ct41);abi-1(RNAi)</i>	32
Figure 9 - <i>mig-10(ct41);abi-1(RNAi)</i> , DIC and fluorescence	32
Figure 10 - <i>mig-10(ct41);unc-53(RNAi)</i> and <i>unc-53(RNAi)</i>	33
Figure 11 - <i>mig-10(ct41);L440(RNAi)</i>	34
Figure 12 - Schematic of expression clone generation	38
Figure 13 - Gel Analysis of PCR Clones	39
Figure 14 - pDONR201 vector map.....	40
Figure 15 - Entry vector generated by recombination event with PCR product.....	41
Figure 16 - MIG-10 does not function cell autonomously in excretory canal outgrowth	44

Table of Tables

Table 1 - Timetable for RNAi feeding.....	21
Table 2 - Table of Primers use to generate AttB-flanked PCR constructs	26
Table 3 - PCR Reaction Mix to generate AttB-flanked clones.....	27
Table 4 - PCR program used to generate AttB flanked clones	27
Table 5 - BP Clonase reaction mixture	28
Table 6: Characterization of <i>C. elegans</i> strains	31
Table 7: Observations of <i>C. elegans</i> strains after RNAi feeding.....	31

Introduction

Neurons are essential cells to the human body. Allowing for control over senses, organ functions, and body movements, neurons comprise both the central and peripheral nervous system. Neurons are the body's means for carrying signals from the outside environment to the brain and out to the body systems. In order for signals to be passed from one neuron to the next in a complete neuronal circuit, proper connections must be made (Bear, Connor, & Paradiso 2001). Much research today involves the study of neuronal connections, including how these connections are established during human development. Connections that do not function properly, a result of developmental mishaps or damage from injury or degeneration by disease, can have grave consequences; faulty neuronal circuits can cause mental retardation, dementia, memory loss, loss of speech, and physical disabilities such as lack of mobility of the limbs. Some common disorders which have spurred studies of the development of neuronal connections include Alzheimer's disease, Parkinson's disease, Cerebral Palsy, Autism, and spinal cord injuries. The exact mechanism by which neurons form, migrate, and then make connections, however, is still unknown.

During development the axon grows by a neuronal growth cone at the tip of the axon (Quinn et. al 2006). The growth cone undergoes cytoskeletal rearrangements and directed cell movements in response to guidance cues (Patel and Van Vactor, 2002; Bear et al, 2003; Chang et. al, 2006; Quinn et. al, 2006). F-actin (actin filaments) and microtubules accumulate asymmetrically in the growth cone according to the guidance cues, resulting in subsequent migration and growth in the direction of the accumulation. Extension of the growth cone proceeds from a meshwork of dense actin known as the

lamellipodium (Figure 1). From this meshwork grows finger-like filopodia made of bundles of actin filaments (Chang et. al, 2006).

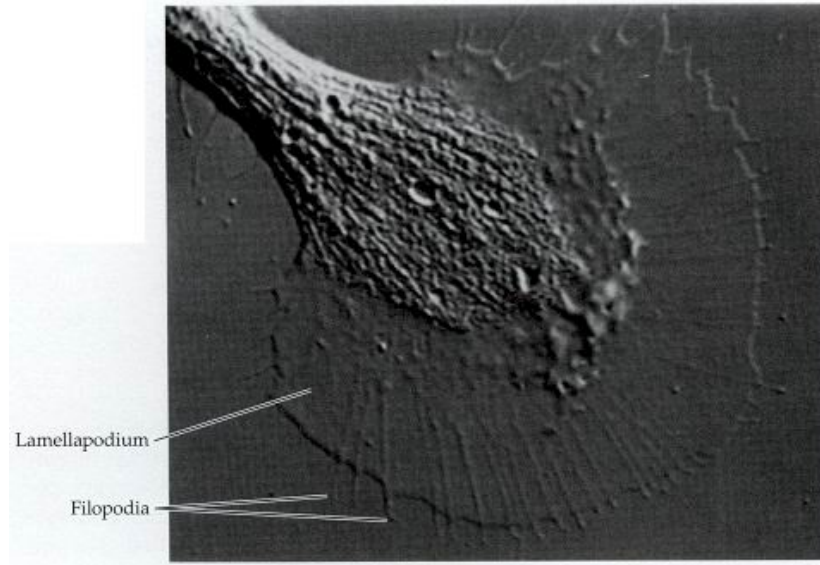


Figure 1 - Axonal Growth Cone with labeled lamellapodium and filopodia
(Purves et. al, 2001)

Central nervous system neurons lack repair mechanisms after a certain age, making spinal cord injuries and late-onset disorders difficult to treat and/or cure. Understanding neurons better, including how they originally migrate during development and the pathways involved in migration, might help to rescue lost signals or rescue repair mechanisms, and to treat damaged neurons. At a molecular level, the genes and translated proteins involved in guidance of axonal growth and migration are pivotal to forming a complete picture of neuronal development. MIG-10, a protein involved in the axonal growth and guidance of neurons in *C. elegans*, was studied for its role in the signal transduction pathway for neuronal growth and migration - specifically, its interactions with other proteins in the pathway.

Caenorhabditis elegans: Model Organism

Caenorhabditis elegans (*C. elegans*), is often used as a model in developmental studies, including genetics. The worms are extremely small, best visible under a microscope, and have a rapid life cycle, which makes them easy to maintain and study. The *C. elegans* genome is mapped extensively, allowing for the mutating and cloning of genes to be commonly used in genetic studies (Manser et. al, 1997). They have 302 neurons of varying classifications, and researchers have been able to isolate and manipulate many of the genes associated with these neurons (Hobert, 2005). The subsequent effects of mutations on neuronal development and migration can be quantified by fluorescence and microscopy due to the translucent nature of the *C. elegans*.

MIG-10

mig-10 was discovered in a genetic screen while looking for disrupted migration of the Canal-Associated Neuron (CAN) in *C. elegans*. In a study by Manser and Wood (1990), mutations in the *C. elegans* genome were isolated and characterized for their involvement in long-range anteroposterior migration of the neurons during development. The neurons of particular interest in this study were CAN, ALM, and HSN, which are some of the very few cells of *C. elegans* which participate in long-range migration. After complementation screening with other known migration defect mutations, it was determined that MIG-10 functioned in a pathway previously unknown to researchers (Manser and Wood, 1990). The protein has been studied extensively for its function in axonal migration and guided growth. One particular *mig-10* allele, *ct41*, is an early stop codon in the coding region, and results in a mutant animal which has incomplete migration of CAN, ALM, HSN, and shortening of the excretory canal (Manser and

Wood, 1990; Manser et. al, 1997). Manser et. al (1997) found, through cloning and molecular characterization of the gene, that *mig-10* encodes two isoforms which contain domains similar to mammalian G-proteins; these were designated *mig-10a* and *mig-10b*. Since then, *mig-10c*, a third isoform, has been discovered. Genetic mosaic analysis revealed MIG-10 functions cell non-autonomously in development of the excretory canal. This means that although mutations in *mig-10* result in truncation of the excretory canal, MIG-10 has been shown to be functioning not in the excretory canal itself, but most likely in the epidermal cells surrounding the excretory canal (Manser et al., 1997). However, because mutations in *mig-10* cause an excretory canal truncation phenotype, it is possible to identify, and quantify the severity of, a *mig-10* mutant simply by analyzing the outgrowth of the excretory canal.

Using differential interference contrast, the effects of MIG-10 mutations on the neurons of interest in *C. elegans* were quantified (Manser et. al, 1997). CAN and ALM neurons, which normally migrate from anterior to posterior in development, appeared to have their migration truncated, as did the HSN neuron that normally migrates from posterior to anterior. Chang et. al (2006) found that mutant *mig-10(ct41)* resulted in axon guidance defects of some of the same neurons. CAN and HSN neurons were both found to have truncated cell migration as well as axon guidance defects, while half the HSN neurons had irregular ventral and lateral neuronal branching. The neurons AVM and ADL showed loss of axonal branching. While it was concluded that MIG-10 functions in proper axonal development and migration, its placement in the pathway for guided migration is being explored.

C. elegans, though a simple organism compared to mammals, have a wide range of genes with homology to those of mammals. MIG-10 is a *C. elegans* homologue to two vertebrate proteins, Lamellipodin (Lpd) and an Lpd-related molecule, RIAM. Both of these proteins, like MIG-10, are known to stimulate lamellipodia formation, and contain several highly conserved regions: a FPPP motif, which is bound by a EVH1 domain found in Ena/VASP proteins involved in actin polymerization; a Ras/Rap GTPase association domain (RA); a lipid binding pleckstrin homology (PH) domain; and a profilin binding proline-rich domain (Boussiotis, 2004; Krause, 2004). The PH domain binds PI(3,4)P₂ phospholipids, a product of PI3K which is the vertebrate homologue to the *C. elegans* protein AGE-1. MIG-10 shares these regions of homology with Lpd and RIAM, and it has been proven that the protein interacts with CED-10/Rac1, a GTPase; UNC-34, an Ena/VASP family protein; and functions in the same pathway as AGE-1/PI3K. MIG-10's exact role in the signal transduction pathway for migration continues to be elucidated as further protein interaction studies are made.

Guidance cues and the function of Mig-10

Previously, studies of the signal transduction pathways leading to axon outgrowth and guidance had focused on the guidance cues and receptors, which were the farthest upstream part of the signal transduction pathway (Patel and van Vacter, 2002) (Yu, et al., 2001). This work determined many different classes of ligands, such as the secreted Netrins, Slits, and Semaphorins, and the cell-surface Semaphorins and Ephrins. It also determined classes of receptors, such as UNC-40/DCC, ROBO, Neuropilin and Plexin, and Eph, which bind each of the classes of ligands respectively. Once the complicated interactions for these receptors and ligands were elucidated, focus shifted to what

happens downstream and trying to determine the complex intracellular pathways, which led to the ultimate goal of axon guidance.

Examination of how guidance cues affect proteins involved in axonal migration has shown that MIG-10 functions downstream of the guidance cue UNC-6/netrin and its receptor UNC-40/DCC, as well as the guidance cue SLT-1 and its receptor Robo (Chang et al, 2006; Quinn, et al., 2006; Quinn, et al., 2008). Genetic analysis confirmed that mutations in MIG-10 enhanced the already noticeable guidance defects caused by the absence of both SLT-1 and UNC-6. When MIG-10 was over-expressed in the absence of UNC-6 and SLT-1, unorganized axonal outgrowth was observed with multiple undirected processes formed. This mutant phenotype was suppressed by addition of either SLT-1 or UNC-6; the axonal process extended from the point of MIG-10 localization, which occurred in attraction to UNC-6/netrin and in repulsion to SLT-1/slit. MIG-10 functions in actin outgrowth-promoting activity and lamellipodia formation, but in order for the axon to be guided toward its intended connection site, guidance cues are needed.

MIG-10 in complex with other proteins

Investigations of the signaling pathway, from the presence of the guidance cues to the accumulation of actin and microtubules and subsequent guided extension of the growth cone, include determining which proteins act in sequence and which act in complex with others. MIG-10 was found to work in conjunction with UNC-34 in guiding axons in response to netrin (Chang et. al, 2006). When a *mig-10;unc-34* double mutant was formed, severe guidance defects of axons were found. Single *unc-34* mutants lacked the formation of filopodia on axonal outgrowths, while the axon still had directed growth with MIG-10 functioning. With both functioning together, UNC-34 allows for filopodial

formation and MIG-10 increases the number of filopodia (Chang et. al, 2006). In the same study MIG-10 was examined for interaction with phosphoinositide-3 kinase (PI3K) AGE-1. Over expression of MIG-10 resulted in excessive growth of axons, while a null mutation of AGE-1 suppressed the excessive outgrowth. This led to the conclusion that AGE-1 acts upstream of MIG-10 in the development of axons. AGE-1 is a regulator of MIG-10 in the guided axon growth for AVM.

MIG-10 is currently being studied for interactions with many proteins both upstream and downstream of lamellipodia formation. Though *C. elegans* is a simple organism, the mechanism by which its neurons migrate is just as complex as that of higher organisms; MIG-10's function is not just limited to lamellipodia formation. The cell non-autonomous expression in cells surrounding the excretory canal suggests that MIG-10 may be important in processes besides simply actin polymerization. In addition, one of the mammalian homologues to MIG-10, RIAM, also functions in cell adhesion – over-expression of RIAM induced cell spreading and lamellipodia formation, as well as integrin activation and cell adhesion. Knockdowns of RIAM reduced actin polymerization (Lafuente et al, 2004). Understanding the function of other proteins in the signal transduction pathway for axonal migration will assist in comprehending exactly how MIG-10 fits into the pathway.

ABI-1

ABI-1 is the interacting protein of interest in this study. Abelson interacting protein-1 (ABI-1) was identified in a yeast two hybrid screen using MIG-10 as the “bait” molecule and a *C. elegans* cDNA library as a collection of “prey”. The screen identified ABI-1 as having a strong *in vitro* interaction with MIG-10 (Gossellin and O’Toole,

2008). ABI-1 is a 476 amino acid, proline-rich protein, which has amino terminus Wave binding (WAB) and syntaxin binding (SNARE) domains, along with a carboxy terminus SH3 domain. ABI-1, *in vivo*, serves several well-characterized functions. First, it is strongly implicated in limiting branching for dendrite extension; when Abi-1 is suppressed using small RNAi, dendrite numbers increase and grow uncontrollably, whereas when Abi-1 is over-expressed it reduces the total number of dendrite branching points (Proepper, et al., 2007). This is possibly due to ABI-1's interactions with, and activity in activating, the WAVE complex (Innocenti et al, 2004). WAVE2 mediates actin nucleation in an Arp2/3 dependent manner, and actively binds Rac-GTP. WAVE1 is maintained in an inactive state in complex with Nap1, PIR121, and HSPC300; Rac-GTP relieves the inhibition, allowing for actin polymerization. The mouse homologue of ABI-1, E3b1, has been shown to be important in cross-talk between Ras and Rac (Scita et. al., 1999), and the activation of Rac; in addition, ABI-1 has been shown as an interactor of the WAVE complex. In a completely unrelated function, ABI-1 has been shown to localize to the nucleus in the presence of certain proteins, and to interact with the Myc/Max complex involved in transcription, which implicates it as having more functions that are integral to the survival of the cell than just actin polymerization and dendrite branching (Proepper, et al., 2007) (Echarri et. al., 2004).

Project goals: Testing ABI-1's interaction with MIG-10

The fact that ABI-1 is a strong interactor with MIG-10 *in vitro* does not implicate it in the same pathway as MIG-10. In order to determine if the interaction is significant, further studies need to be done *in vivo* using both *mig-10* and *abi-1 C. elegans* mutants.

Since ABI-1 has many functions *in vivo*, it follows that a null mutation in the *abi-1* gene would potentially cause embryonic or early larval death in *C. elegans*. There is a weak *abi-1* allele available, however the phenotype is very mild; therefore, it is preferable to use RNA interference to view the effects of lowered levels of ABI-1. RNAi works by a single-stranded segment of RNA binding to a post-transcriptional RNA, targeting the complex for degradation and knocking down expression of the gene (Fire et al., 1998). Since ABI-1 is known to interact with MIG-10 *in vitro*, if the interaction is significant *in vivo* similar effects should be seen with *abi-1 RNAi* as with a *mig-10* null mutation, specifically in the truncation of the excretory canal. In addition, if MIG-10 and ABI-1 function in the same pathway with no overlapping functions, a worm with both decreased function of both ABI-1 and MIG-10 should show a phenotype no worse than that of *mig-10* or *abi-1* individually.

Biochemical Analysis of the MIG-10/ABI-1 Interaction

Detecting protein-protein interactions is one of the staples of biochemical analysis – finding physical interactors of proteins is often the first step in determining the order of signaling pathways in living cells (Phizicky and Fields, 1995). However, each system has drawbacks, and it's often preferable to confirm results in multiple systems.

Yeast Two Hybrid System

Previous studies of the ABI-1/MIG-10 interaction were done in the yeast two hybrid system (Gossellin and O'Toole, 2008). This system relies on the presence of two different domains in transcriptional activation: the DNA binding domain, fused to the “bait”, and the activation domain, fused to the “prey”. Each domain is fused to a protein of interest, two proteins thought to physically interact, and co-expressed in yeast. The

DNA binding domain binds selectively to the promoter region of a reporter gene, and physical interaction between the two proteins brings the activation domain within close proximity of the DNA binding domain. The proximity of the two allows for transcription and expression of the reporter gene. This is a very sensitive assay, and allows for detections of interactions that often can't be detected by any other method; however, there are some problems with the system. First of all, the protein needs to be able to localize to the nucleus, otherwise it is not possible for it to interact with the reporter gene. Proteins that are normally involved in transcriptional activation can sometimes activate expression of the reporter gene without interaction with the prey protein, leading to a background of self-activation which may cause false positive results. In addition, since the yeast cell is a low-level eukaryotic organism, proteins that rely on post translational modifications for their interactions often can't be detected as interacting.

ABI-1 and MIG-10 were determined to be physical interactors, but over a fairly high background signal due to self-activation of the MIG-10A isoform; the MIG-10C isoform had such high levels of self-activation that no interactions could be detected. Therefore, it is important to confirm the results in another system.

Co-immunoprecipitation

The method of analysis chosen to confirm the interaction was co-immunoprecipitation (Co-IP) of the target proteins in insect cells using fusion tags as markers. The principle behind Co-IP is simple – proteins of interest are co-expressed in a cell line, in this case insect cells. Once the cells have had time to express the protein, they are lysed and pelleted; this allows for the soluble proteins to remain in solution,

while all insoluble proteins and cell debris are removed. The lysate is then probed with antibodies to each individual protein, one at a time. If the proteins are strong physical interactors, then detection by either antibody should show both proteins of interest.

There are also problems with this method of detection. The Co-IP system can only be used with strong interactors, since weak interactions will be disrupted by the cell lysis and subsequent purification steps. However, there is no problem with self-activation or false positives, and since insect cells are higher eukaryotes they have more efficient post translational modifications.

Project Goal: Testing MIG-10's Physical Interaction with Other Proteins

The yeast two hybrid screen pulled out three strong interactors of MIG-10: ABI-1, ARX-3, and LIN-53. The project goal was to clone constructs for each of these proteins into vectors appropriate for use in an insect cell co-IP system. Then, time permitting, all three MIG-10 isoforms (A,B,C) plus the RAPH domain (which is a candidate for the interacting domain) would be expressed fused to a GFP tag; ABI-1, ARX-3, and LIN-53 would be expressed fused to a 6xHis tag. Both tags can be detected by specific antibodies. If a physical interaction is seen between any of the combinations of proteins, then co-expression and immunoprecipitation of one of the proteins followed by denaturing western blot analysis should show bands which represent each of the different proteins. If a physical interaction is not seen, then the western will show only a single band representing the protein precipitated by the corresponding antibody.

Methods

RNAi Feeding Protocol

The procedures followed in RNAi feeding were adapted from Stringham and Ahringer lab protocols (Ahringer, 2003 & Schmidt et. al, 2009). The methods reflect the optimal procedures used over the course of multiple RNAi feedings. See Appendix A for RNAi diagram.

Preparation of RNAi Plates

The RNAi plates consisted of NGM agar, and IPTG and carbenicillin were added after autoclaving to final concentrations of 1mM IPTG and 25ug/mL carbenicillin. This yielded approximately 36-48 plates. The newly poured plates were allowed to set, and stored at 4°C to prohibit any degradation of the IPTG at room temperature. Following the procedures of the Ahringer and Stringham labs, the plates were allowed to set for at least 3 days before being used.

Inoculation and Seeding of RNAi bacterial strains

RNAi strains were streaked onto LB + 50ug/mL Amp and 12.5ug/mL Tet plates. Using sterile pipet tips, single colonies were picked to sterile 15mL conical tubes containing 5mL LB + 50ug/mL Amp. The inoculated cultures were placed in a rotating drum in a floor incubator overnight (12-15 hours maximum) at 37°C.

After 12-15 hour incubation, the cultures were spun at 1000 x g for 5 minutes in a balanced table top centrifuge to concentrate them. While the cultures were spinning, the RNAi plates to be seeded were removed from the refrigerator to warm slightly before seeding. After the cultures had been spun, all but 1mL supernatant was removed by sterile pipettes. The bacterial pellet was re-suspended in the 1mL of supernatant by vortexing. For

each RNAi strain, 3 labeled RNAi plates were seeded with 3-5 drops of cultured RNAi bacteria using sterile Pasteur pipettes. Plates were allowed to set in sterile hood overnight, with the blower on to facilitate drying.

Transfer of worms to RNAi plates

C. elegans at the L4 stage in their life cycle were transferred from non starved plates to the seeded RNAi bacterial plates. Each plate was labeled with the strain of *C. elegans* added and the number of L4s transferred. 4-6 L4s were transferred in attempts to have large numbers of progeny for quantification. Care was taken to not cross-contaminate the different RNAi plates. After the transfer, the plates were kept at 25 °C for 30 hours.

After 30 hours at 25°C, the *C. elegans* on the primary plates (then gravid adults), were transferred to secondary RNAi plates. These plates were prepared in the same manner as the primary plates, in a timetable that had them ready for the new transfer (see Table 1 for the timetable used). Plates were labeled such that transfers could be followed from primary plates to each corresponding secondary plate. After the transfer to the secondary plates, both primary and secondary plates were put at 25°C for 48 hours.

Starting at 40 hours, the plates were checked every 2-4 hours for F1 progeny at the L4 stage. L4s were quantified as detailed below. Sometime between 40 and 48 hours, 4-6 L4s from each plate were transferred to tertiary plates, prepared ahead of time such that they would be ready at the time of transfer (see Table 1 for the timetable). Labeling continued to follow transfers from secondary to corresponding tertiary plates. These plates were put at 25°C for 72-78 hours.

Starting at 68 hours, the plates were checked every 2-4 hours for F2 progeny at the L4 stage. L4s were quantified as detailed in the next section. No additional transfer took place.

Table 1 - Timetable for RNAi feeding

Day	Time*	Task	Days/Hours to set	Temperature
3-4 days before start	whenever	Prepare NGM plates	4-5 Days	refrigerator
	whenever	Prepare strains for Day 3 transfer	3-4 days	20°C
Day 1	8:00pm	Inoculate 1° cultures	12-15 hours (min-max)	37°C
Day 2	8:00am	Seed 1° plates	24-30 hours (max)	Room temp
Day 3	6:00am	Inoculate 2° cultures	12-15 hours (min-max)	37°C
	11:00am	Transfer P0 L4s to 1° plates	30 hours	25°C
	6:00pm	Seed 2° plates	24-30 hours (max)	Room temp
Day 4	5:00pm	Transfer P0 adults to 2° plates	40-48 hours	25°C
	6:00pm	Inoculate 3° plates	12-15 hours (max)	37°C
Day 5	8:00am	Seed 3° plates	24-30 hours (max)	Room temp
Day 6	11:00am	Transfer F1 L4s to 3° plates	68-72 hours	25°C
Day 6	11:00am	Score F1 L4s from both 1° and 2° plates		
Day 9	9:00am	Score F2 L4s		

*These are the times used in this trial. The important section to follow is the days/hours to set, as time availability in different labs might vary.

Preparing slides for scoring of F1s and F2s from RNAi feeding

L4s were picked from the primary, secondary, and/or tertiary plates as F1s or F2s. Two methods of making slides for quantification were used.

- 1) L4s were picked directly to an agarose azide slides. Premade 2 ml aliquots of 2% agarose were heated to liquid state in a water bath. 20µL of 1M sodium azide was added to the liquid agar, vortexed, and 2 drops pipetted to a blank slide, and another slide was immediately placed perpendicularly on top to make a pad of agarose. L4s from a particular set of plates were transferred to spotted NGM plates. 3µL of M9

was added to the dry agarose/azide pad on the slide. Up to 13 worms were picked directly from the spotted NGM plates to the drop of M9 on the slide, after which a coverslip was quickly added to prohibit the M9 from evaporating and keep the worms in a lateral orientation. This was repeated for each set of RNAi.

2) L4s transferred to slide by washing plates. Agarose slides prepared as above. L4s from a particular set of plates were transferred to spotted NGM plates. A few drops of M9 were added to the NGM plate of L4s, swished gently, and the liquid pipetted into a 1.5mL Eppendorf tube. The worms were allowed to settle to the bottom of the Eppendorf. As many worms as possible were pipetted in 3-5 μ L of M9 to the agarose slide. A coverslip was added quickly and the slide labeled according to the RNAi and strain of *C. elegans*. This was repeated for each set of RNAi.

Quantification/Scoring of F1s and F2s from RNAi feeding

The slides were examined under a compound microscope. The worms were each observed under differential interference contrast (DIC), first to identify the age of the worm, and then to determine where the gonad arms began and ended. The fluorescence was used to focus on and quantify the length of the excretory canal. A grid system was used in quantifying the region of the body in which the *C. elegans* excretory canal ended (Figure 2). The strain of worm, RNAi bacterial strain, age of worm, and region of truncation for both of two processes for the excretory canal were recorded. In the case that only one process could be found, the region of truncation was recorded for just one process. Each worm was assigned a total truncation value equal to the sum of that recorded for the two processes, or twice the truncation value for the process if only a single process was observed.

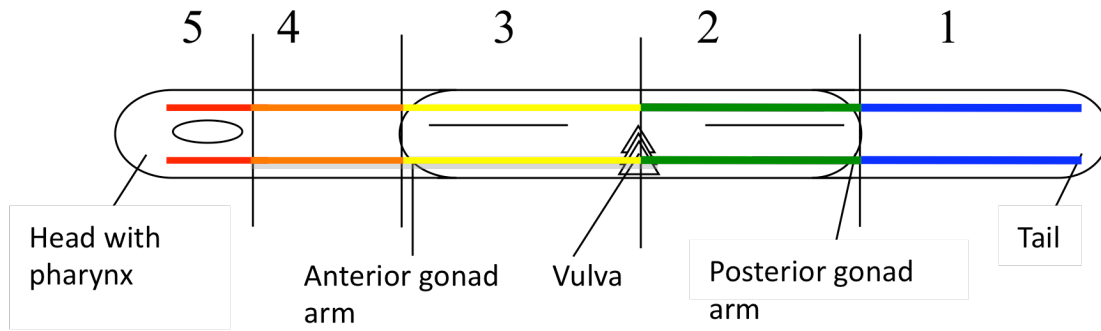


Figure 2 - Schematic of regions of worms for quantification of truncation

(Adapted from Schmidt, et. al., 2009).

Statistical Analysis of Different Generations

Since each experiment was analyzed on three different RNAi plates, chi-square analysis was used to determine if data could be combined across plates. Data were collected as shown in Figure 3, where the numbers of worms displaying each summed truncation (region) are shown in each column, and each plate is shown in each row:

Experiment	Plate	10	9	8	7	6	5	4	3	2	totals
<i>abi-1(RNAi)</i>	Primary	0	0	0	0	1	2	8	15	31	57
	Secondary	0	0	0	0	0	0	1	10	21	32
	Tertiary	0	0	0	0	0	0	2	5	24	31
Totals		0	0	0	0	1	2	11	30	76	120

Figure 3 - Sample table for data consolidation

Counting the number of worms which truncated in each region for each of the primary, secondary, and tertiary plates.

A chi-square value was determined for each plate (primary, secondary, tertiary) using the following equation:

$$X^2 = \sum_i \frac{(O_i + E_i)^2}{E_i}$$

Equation 1 – Chi-square formula for individual conditions

Where O_i is equal to the observed value for each truncation value for that particular plate, and E_i is calculated as:

$$E_i = \frac{\text{plate_total} \times \text{region_total}}{\text{grand_total}}$$

Equation 2 - Calculation of expected value for chi-square analysis

The chi-square values for each individual plate were added together, and a p value determined by comparison against a table of threshold values using the following equation to determine the degrees of freedom (DF) of the entire experiment. If a column or row contained only 0's, it was not included in the chi-square calculation for that experiment.

$$DF = (\text{plates} - 1) \times (\text{regions} - 1)$$

Equation 3 - Calculation of degrees of freedom for chi-square analysis

The null-hypothesis for this experiment was that there is no difference between individual plates. If $p > 0.05$, then data could be combined across plates; if $p < 0.05$, then the individual plates were too different for data to be combined.

Statistical Analysis of Different Strains

In order to determine if the differences in excretory canal truncation were statistically significant between different experimental conditions, chi-square analysis was done (Figure 4). The data were collected as follows, using the combined totals (where applicable) from each individual strain:

Comparison	10	9	8	7	6	5	4	3	2	Totals
<i>mig-10(ct41);abl-1(RNAi)</i>	52	7	28	6	18	0	0	0	0	111
<i>mig-10(ct41);L440(RNAi)</i>	11	11	48	42	51	0	0	0	0	163
Totals	63	18	76	48	69	0	0	0	0	274

Figure 4 - Sample table for chi-square analysis for strain comparison

The individual strains were compared using the same methods as above. The null hypothesis for these comparisons was that there is no difference between the different strains; if $p < 0.05$,

it was assumed that the difference seen between the strains was significant, and if $p > 0.05$, then the difference seen between strains was due to biological variation and not significant.

PCR for generating Att Sites

Polymerase Chain Reaction was done using the following primers (Table 2) and protocol (Table 3, Table 4) to generate AttB1 sites on 5' and AttB2 sites on 3' ends of genes of interest.

Table 2 - Table of Primers use to generate AttB-flanked PCR constructs

All primers that were used in PCR reactions to generate AttB-flanked constructs are listed above; in the forward constructs, the first 30 bases are the AttB site, up through the first ATG, after which follows the part that binds to the gene. In the reverse constructs, the first 27 bases are the AttB site.

Primer Name	Mt	Description	Sequence
abiForatt	67	Abi-1 AttB Forward Primer	GGG GAC AAC TTT GTA CAA AAA AGT TGG AAA ATG AGT GTT AAT GAT CTT CAA GAG
abiRevatt	70	Abi-1 AttB Reverse Primer	GGG GAC AAC TTT GTA CAA GAA AGT TGG TAC TGG AAC TAC GTA GTT TCC AG
lin53foratt	70	Lin-53 AttB Forward Primer	GGG GAC AAC TTT GTA CAA AAA AGT TGG AAA ATG GCC ACT CTT GAA GAT GGA AC
lin53revatt	71	Lin-53 AttB Reverse Primer	GGG GAC AAC TTT GTA CAA GAA AGT TGG CTG TTG TCT CTC TAC CAC ATC G
arx3foratt	70	Arx-3 AttB Forward Primer	GGG GAC AAC TTT GTA CAA AAA AGT TGG AAA ATG ACC AAC AGA ATC GTC TCA TGT TC
arx3revatt	71	Arx-3 AttB Reverse Primer	GGG GAC AAC TTT GTA CAA GAA AGT TGG GAC GAG TGA TGG GTG ATT CTT C
mig10aforatt	70	Mig-10a AttB Forward Primer	GGG GAC AAC TTT GTA CAA AAA AGT TGG AAA ATG GAC ACT TAC GAC TTC CCG
mig10bforatt	71	Mig-10b AttB Forward Primer	GGG GAC AAC TTT GTA CAA AAA AGT TGG AAA ATG TAT CAC GAT CGA CGG CG
mig10cforatt	71	Mig-10c AttB Forward Primer	GGG GAC AAC TTT GTA CAA AAA AGT TGG AAA ATG GAC AGT TGC GAA GAG GAA TGC
mig10revatt	71	Mig-10 AttB Reverse Primer	GGG GAC AAC TTT GTA CAA GAA AGT TGG ACA CTC CAT GGT TGC CAT TTT CTC
mig10RAPHforatt	71	Mig-10 RAPH AttB Forward Primer	GGG GAC AAC TTT GTA CAA AAA AGT TGG AAA ATG GGT GAC TCA AGT TCA ACT GAA TCC
mig10RAPHrevatt	70	Mig-10 RAPH AttB Reverse Primer	GGG GAC AAC TTT GTA CAA GAA AGT TGG CAA ACT ATG TGG AAC TTC AGA AAT AGC

Table 3 - PCR Reaction Mix to generate AttB-flanked clones

The reaction mixed above was used to generate each AttB flanked gene of interest; the mix is the result of rounds of optimization. The 4ng DNA is an estimate based on gel bands; generally, a 1:100 dilution of Qiagen Miniprep DNA is sufficient.

Reagent	Final Concentration
Plasmid DNA	4ng
ThermoPol Buffer	1x
dNTPs	200uM
5' Primer	0.4uM
3' Primer	0.4uM
Vent Polymerase	0.56 Units
Final Volume	50uL

Table 4 - PCR program used to generate AttB flanked clones

The program is based on a standard program for Vent Polymerase, and optimized for the long primers used in the extension.

Step	Temp	Time
Denaturation	95	5 min
20 Cycles	Denature	95 30 sec
	Annealing	57 30 sec
	Extension	72 90 sec
Final Extension	72	5 min
Storage	4	∞

All PCR products were analyzed by gel electrophoresis, 1% agarose gels in 1x TAE buffer, run for 1-1.5 hours at 100V.

BP recombination reaction

The recombinase reaction mixture (Table 5) was incubated for 1hr at 25°C to allow for the recombination event, and then stopped with 2uL proteinase K.

Table 5 - BP Clonase reaction mixture

Reagent	Final Concentration
pDONR201	~5-6nM
AttB Gene Specific PCR	~5-6nM
BP Clonase	2uL
Final Volume	10uL

Transformation of competent cells

Competent cells were transformed with the plasmids resulting from the BP reaction, or with DNA from Qiagen minipreps. 1 uL clonase reaction (or 1uL) was added to 50uL Top-10 One-Shot Competent *E.coli*®, and allowed to incubate 30min on ice. The cells were then heat shocked for 30sec at 42°C. 400uL SOC recovery media were added, and the cells were incubated 1hr at 37°C. After recovery, 50uL and 200uL were plated on LB+50ug/mL Kan plates, and incubated 24hrs at 37°C.

Single colonies (3-5 per construct) were grown up in 5mL LB+50uG/mL Kan for 12-24hrs at 37°C.

Isolation of plasmid DNA

Plasmid DNA was isolated using the QIAprep Spin Miniprep© protocol. Cells were pelleted at ~1400 x g for 5 min, and then resuspended in 250uL Buffer P1. 250uL Buffer P2 was then added, mixed thoroughly. 350uL Buffer N3 was added, and the tube inverted 4-6 times to ensure proper mixing. The mixture was centrifuged 10 min at ~14,000 x g, and the supernatant was applied to a QIAprep spin column. The column was spun for 30-60s at 14,000 x g, and the flow-through discarded. 0.5mL Buffer PB was applied to the column, spun for 30-60s at 14,000 x g, and the flow-through was discarded. 0.75mL Buffer PE was applied to the column, spun for 30-60s at 14,000 x g, and the flow-through was discarded.

The column was spun for an additional 1min, and the flow-through was discarded. Finally, 50uL Buffer EB was applied to the column, the column was placed in a 1.5mL eppendorf tube, allowed to sit for 1 min, and then spun for 1-2min at 14,000 x g. DNA was stored at 4°C.

Results

Given the observed ABI-1/MIG-10 interaction *in vitro* with a yeast two hybrid system, RNAi expression knockdown was used to establish if the interaction was relevant to outgrowth of the excretory canal *in vivo*. To determine whether ABI-1 affected excretory canal outgrowth on its own, both *abi-1(tm94)* mutant animals and animals treated with *abi-1(RNAi)* were examined. To determine whether various proteins interacted with *mig-10(ct41)* in excretory canal outgrowth, several different RNAi constructs were used in combination with *mig-10(ct41)* mutant animals

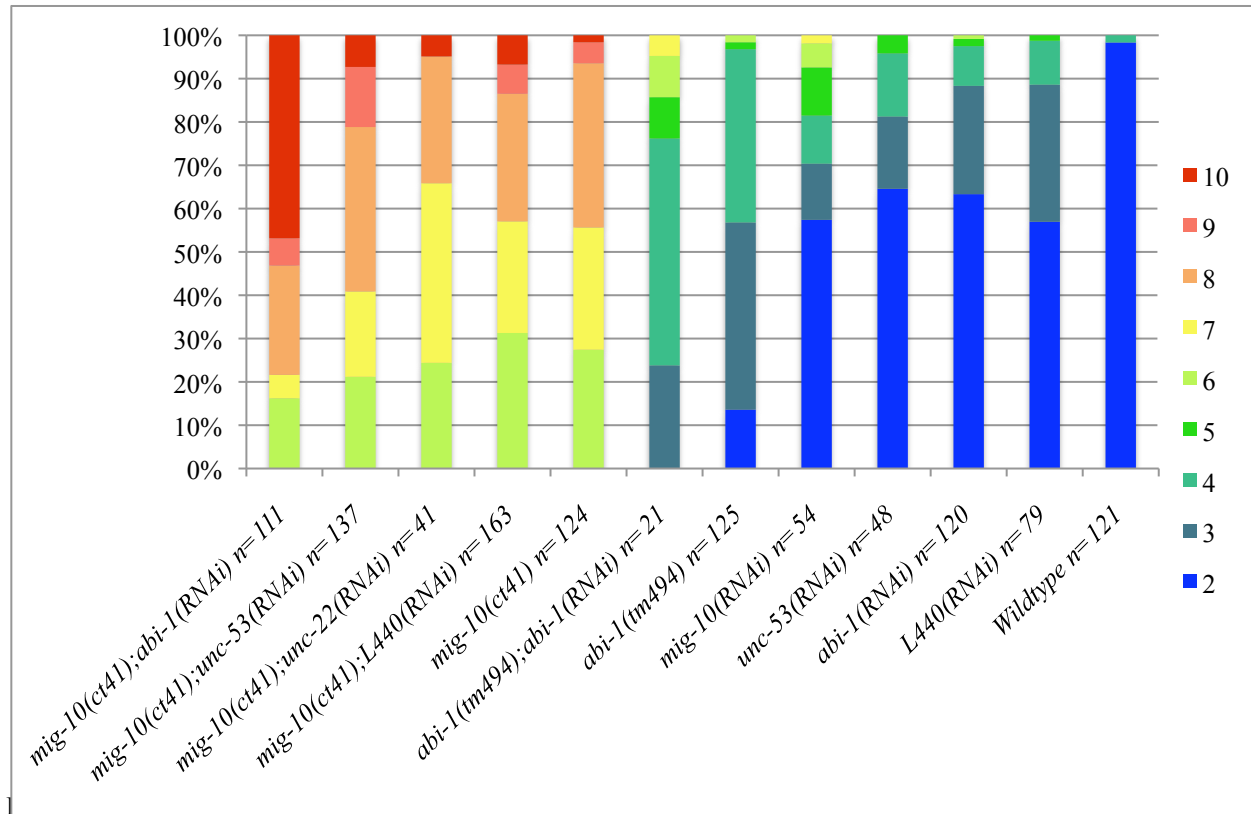
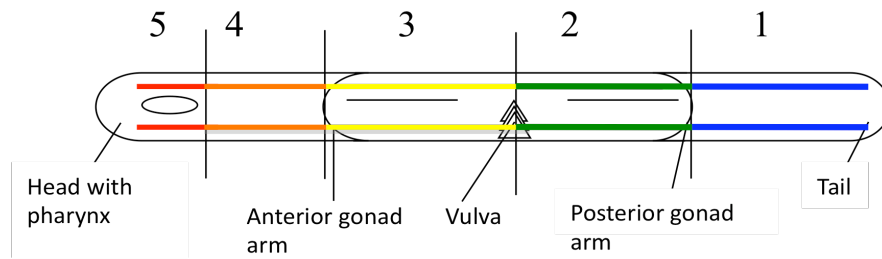
In all cases, L4 or young adult worms were used, ensuring that both the vulva and the gonad were fully formed and that the excretory canal was at its longest point and had not yet “snapped back,” as is common in adult worms. General observations of worm phenotypes observed with a visible light dissecting microscope are summarized in Tables 6 and 7. Analysis of the excretory canal was performed using a combination of differential interference contrast (DIC) and fluorescence. Each process of the worm was analyzed for severity of truncation based on which region of the worm the excretory canal outgrowth terminated (Figure 5). The numerical representations of truncation for both processes were added together to more accurately represent the overall truncation seen in the worm. The sum representations of excretory canal truncation for each worm and RNAi pairing were graphed for comparison of truncation (Figure 5).

Table 6: Characterization of *C. elegans* strains

Text Reference	Strain name	Genotype	Allele	Mutation	Characteristics
Wild Type	BC06288	<i>siIs10089</i>	Wild Type	N/A	No deformities, large brood size
<i>mig-10(ct41)</i>	RY108	<i>mig-10(ct41);bgIs312</i>	amorphic	C-terminal truncation	Cleft head, pVul, Egl, rate brood size
<i>abi-1(tm494)</i>	VA74	<i>abi-1(tm494);sIs10089</i>	hypomorphic	C-terminal truncation	pVul, moderate brood size

Table 7: Observations of *C. elegans* strains after RNAi feeding

Genotype	RNAi	Observations
<i>mig-10(ct41);bgIs312</i>	<i>abi-1</i>	Distended Vulva; clefts; Egl; decreased brood size; no live F2 progeny
<i>mig-10(ct41);bgIs312</i>	<i>unc-53</i>	Distended vulva; Egl; clefts; moderate brood size
<i>mig-10(ct41);bgIs312</i>	<i>L440</i>	Distended vulva; clefts; large brood size
<i>abi-1(tm494);sIs10089</i>	<i>abi-1</i>	Moderate brood size
<i>sIs10089</i>	<i>abi-1</i>	No apparent deformities; moderate brood size
<i>sIs10089</i>	<i>unc-53</i>	No apparent deformities; moderate brood size
<i>sIs10089</i>	<i>L440</i>	No apparent deformities; large broods



Animal genotypes and arrays follow the notation described in Table 2. The x-axis refers to animals by background genotype; RNAi strain. Worms without a noted background are wild type. The two excretory canal scores were added together, giving each worm an overall truncation. Colors move from blue to red across the visible spectrum, with blue representing little to no truncation (essentially wild-type), and red representing severe truncation (little to no excretory canal outgrowth). The transgene marking the excretory cell was *bgIs312* for strains containing *mig-10(ct41)*, and *sIs10089* for all other strains.

***abi-1* has a small, but very significant effect on excretory canal outgrowth**

Quantification of the animals showed that in the wild type animals, the excretory canal typically reached region 1 of the worm, giving an overall score of 2, or representation of full extension of the excretory canal (Figures 5 and 6A). In contrast, *abi-1(tm494)*

mutants (Figure 6B) and *abi-1(tm494);abi-1(RNAi)* (Figure 7) animals generally showed truncation of the excretory canal in region 2 of the worm, resulting in typical overall scores of 2-4. Interestingly, *abi-1(RNAi)* of wild-type worms did not significantly affect the overall extension of the excretory canal compared to wild-type worms fed on *L440(RNAi)* ($p=0.766$), but *abi-1(tm494)* did show significant truncation compared to wild-type with *L440(RNAi)* (Figure 5; $p<0.0001$). *abi-1(tm494);abi-1(RNAi)* also showed significant effects in extension of the excretory canal when compared to *abi-1(tm494)* mutants not fed on RNAi ($p=0.0016$). These data support the idea that the ABI-1 does in fact function in the outgrowth of the excretory canal and thus is useful in analysis of interaction with *MIG-10;abi-1(RNAi)*, however, does not seem to have a measurable effect on its own.

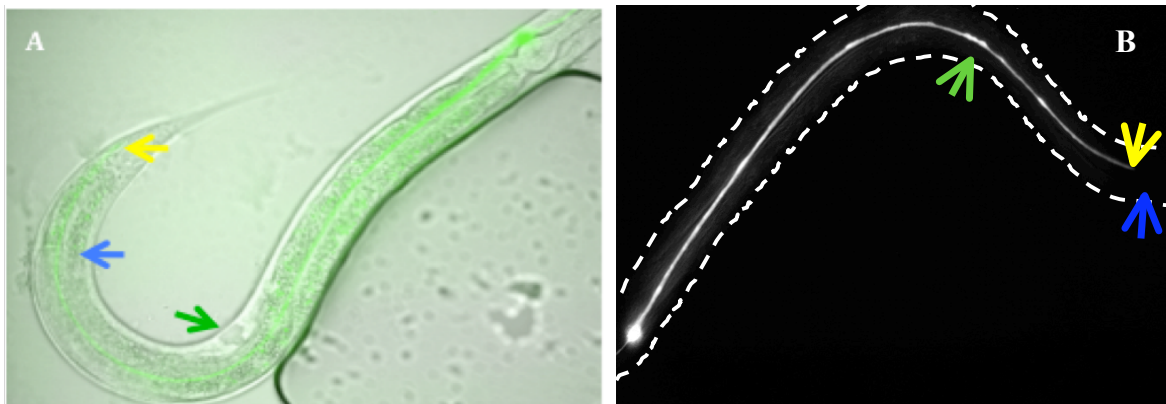


Figure 6 - Wildtype and *abi-1(tm494)* mutant

- A) DIC/Fluorescence merge. Wild type. Anterior to right, yellow arrow marks end of excretory canal, blue marks end of gonad arm, green marks vulva. Excretory canal extends to region 1.
- B) Fluorescence. *abi-1(tm494)* mutant. Oriented anterior left. Excretory canal truncation in region 2. Arrows as in A.

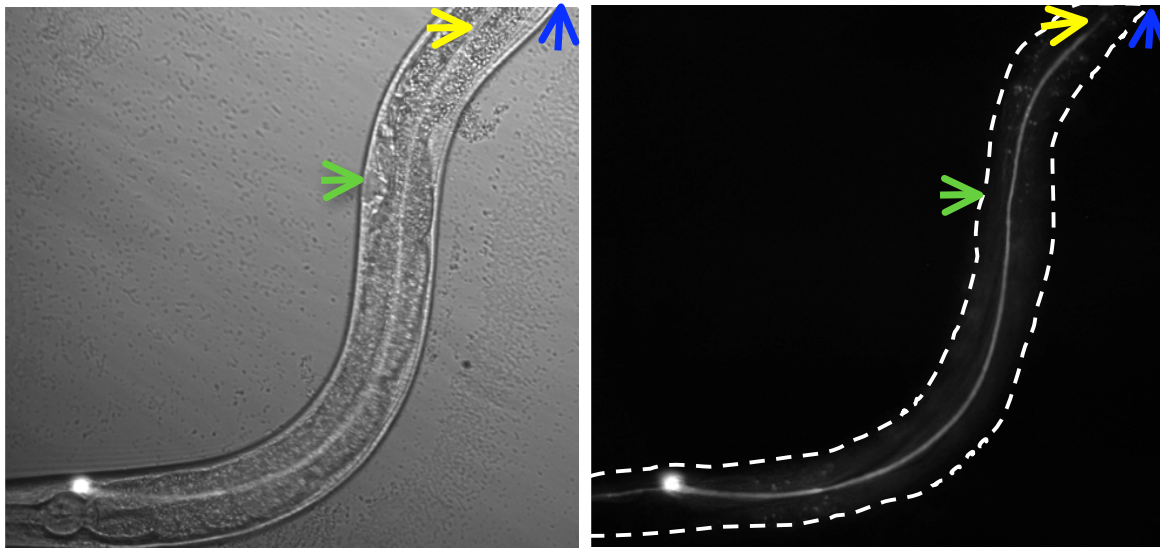


Figure 7 - *abi-1(tm494);abi-1(RNAi)*

Left, DIC; Right, fluorescence. Both oriented with anterior to left. Excretory canal truncates in 2 region. Arrows as in Figure 6.

***abi-1* and *mig-10* show a genetic interaction**

Similar to wild type and *abi-1(tm494)* mutant animals, *mig-10(ct41)* mutants were characterized by quantification of excretory canal outgrowth. *mig-10(ct41)* animals typically showed truncation of the excretory canal in the 3 and 4 regions of the worm, with some variable worms having truncation in region 5 (Figures 5 and 8A). It was found that the *mig-10;abi-1(RNAi)* worms (Figures 8B and 9) had a more severe phenotype than both *mig-10(ct41)* and *mig-10(ct41);L440(RNAi)* worms (Figure 5; both $p < 0.0001$). In addition, it was observed that these animals had smaller numbers of live progeny, and F1 worms (after one generation of RNAi feeding) were unable to lay viable eggs (Table 7). These data support the theory that the ABI-1 and MIG-10 proteins are not simply in the same pathway, but do interact genetically for excretory canal outgrowth.

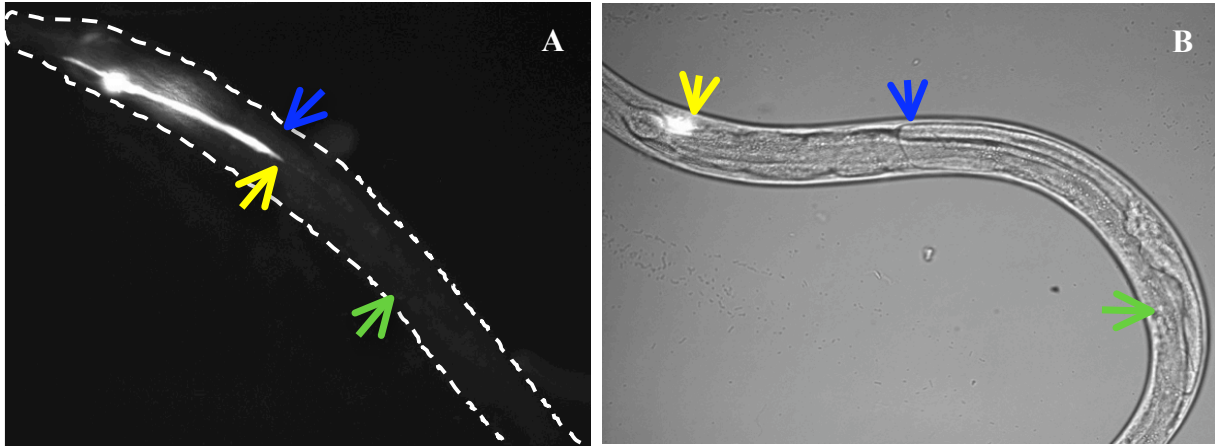


Figure 8 - *mig-10(ct41)* and *mig-10(ct41);abi-1(RNAi)*

- A) *mig-10(ct41)* mutant. Oriented anterior to the left. Excretory canal truncation in 4 region. Arrows as in Figure 6.
- B) *mig-10(ct41);abi-1(RNAi)*. Oriented anterior to the left. Excretory canal truncates in 5 region. Arrows as in Figure 6.

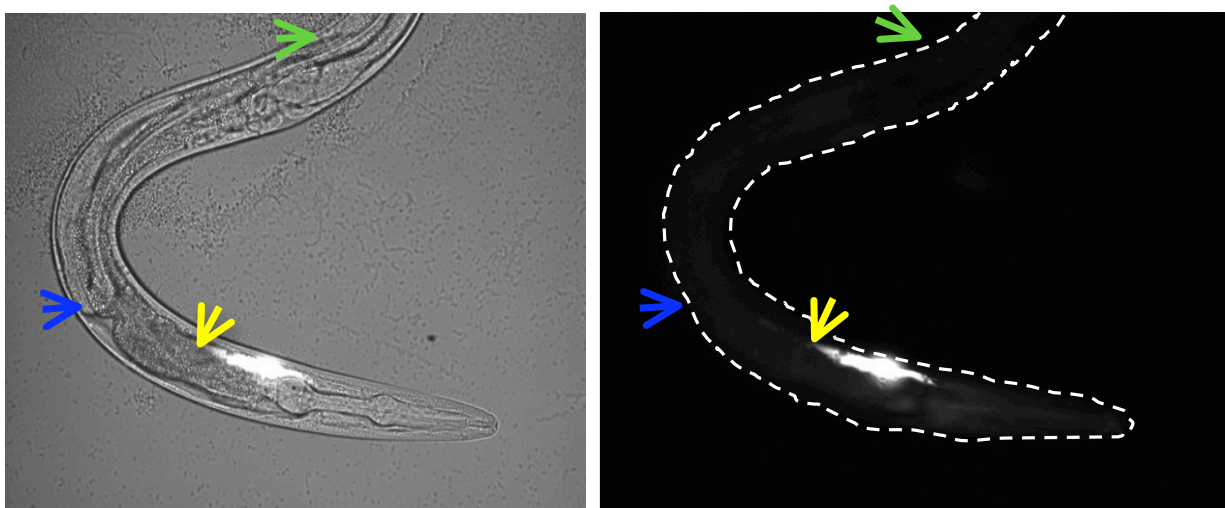


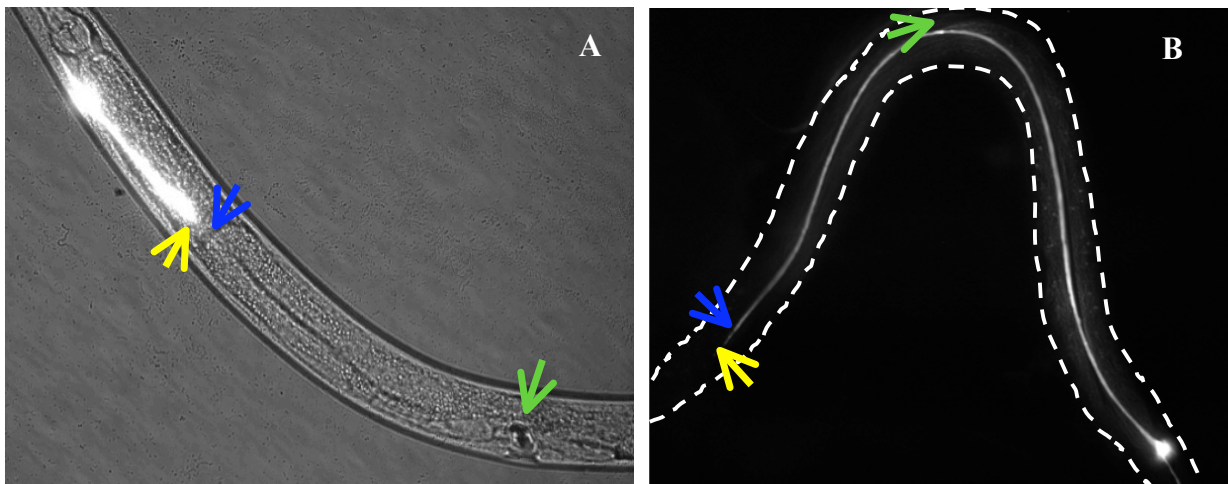
Figure 9 - *mig-10(ct41);abi-1(RNAi)*, DIC and fluorescence

Left, DIC; Right, fluorescence. Both oriented anterior to the right. Excretory canal truncates in 4 region. Arrows as in Figure 6.

unc-53* shows a borderline genetic interaction with *mig-10

Since UNC-53 and ABI-1 are believed to be in the same pathway (Schmidt et. al, 2009), *unc-53* might be expected to also show a genetic interaction with *mig-10* similar to *abi-1* interaction with *mig-10*. This theory was tested by creating *unc-53* expression knockdown by RNAi in *mig-10(ct41)* worms. Surprisingly, in analysis of *mig-10(ct41);unc-*

53(RNAi) worms, it was found that there was only a borderline significant increase ($p=0.0504$) in the severity of truncation of the excretory canal compared to *mig-10(ct41);L440(RNAi)* animals (Figure 5, Figure 10A). This suggests that UNC-53 and MIG-10 may in fact function in the same pathway. However, *unc-53(RNAi)* on its own in wild type animals had no significant effect on the excretory canal (Figure 5; $p=0.218$; Figure 10B), suggesting that there could have been a technical problem with the *unc-53 (RNAi)*, since *unc-53* mutants previously showed fairly severe truncation (Schmidt et al., 2009).



- A) *mig-10(ct41);unc-53(RNAi)*. Oriented anterior to the left. Excretory canal truncates in the 4 region. Arrows as in Figure 6.
 B) *unc-53(RNAi)*. Oriented anterior to the right. Excretory canal extends to region 1. Arrows as in Figure 6.

Controls used to show genetic interactions between proteins

To show the specificity of the genetic interaction between *mig-10(ct41)* and *abi-1(RNAi)*, controls were performed using the empty RNAi vector (L440) and an unrelated RNAi construct (*unc-22*). Analysis of *mig-10(ct41);L440(RNAi)* worms (Figure 11) showed no increased severity in phenotype over *mig-10(ct41)* worms ($p=0.16$); this shows that the presence of the RNAi vector had no effect on the truncation of the excretory canal and thus

all RNAi variables for *mig-10(ct41)* worms were compared to *mig-10(ct41);L440(RNAi)*. In order to test whether an unrelated RNAi construct would have any side effect in the excretory canal, *mig-10(ct41)* worms fed on *unc-22(RNAi)* were analyzed. UNC-22 is not believed to have any function in the excretory canal, but rather through RNAi expression knockdown has a strong twitcher phenotype. The worms were observed as having a strong twitch, which identified the RNAi as a functional construct. There was no increase in the severity of the phenotype in the *mig-10(ct41);unc-22(RNAi)* worms over *mig-10(ct41);L440(RNAi)* (Figure 5; $p=0.181$). These data show that the increased effect seen with *abi-1(RNAi)* was not just an artifact of a functional RNAi having an effect on excretory canal outgrowth.

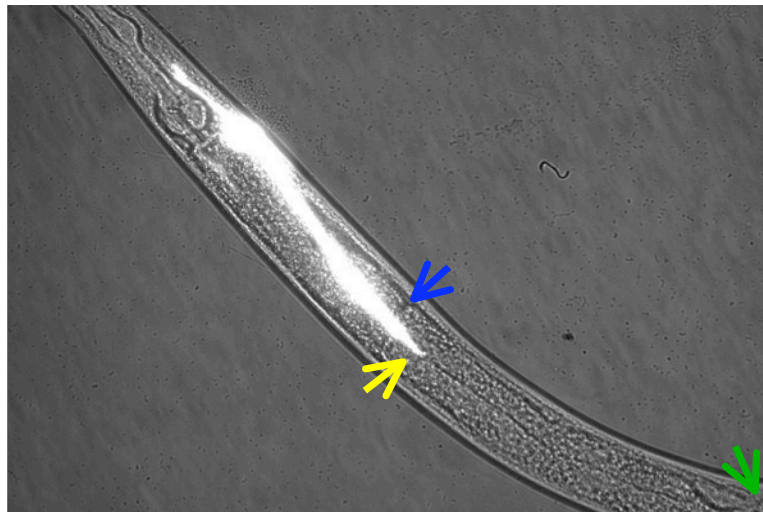


Figure 11 - *mig-10(ct41);L440(RNAi)*

Oriented anterior to the left. Excretory canal truncates in region 3. Arrows as in Figure 6.

Preparation of vectors for Co-immunoprecipitation experiments

In order to confirm the interaction observed between MIG-10 and ABI-1, LIN-53, and ARX-3 previously observed in the yeast two hybrid system, an effort was initiated to transfer the constructs obtained from the previous yeast two hybrid experiments (O'Toole and Gossellin, 2008) into an insect expression system for eventual co-immunoprecipitation.

Generation of an Expression Vector

The Gateway System[®] from Invitrogen was used to generate the intermediate vectors leading to the creation of an appropriate expression vector for each construct. The Gateway[®] system uses Att sites for recombination of select sequences into clones; AttB+AttP → AttL, and AttL+AttR → AttB. Clonase, a proprietary enzyme, was used to catalyze recombination reactions between specific Att sites. The overall strategy is shown in Figure 12.

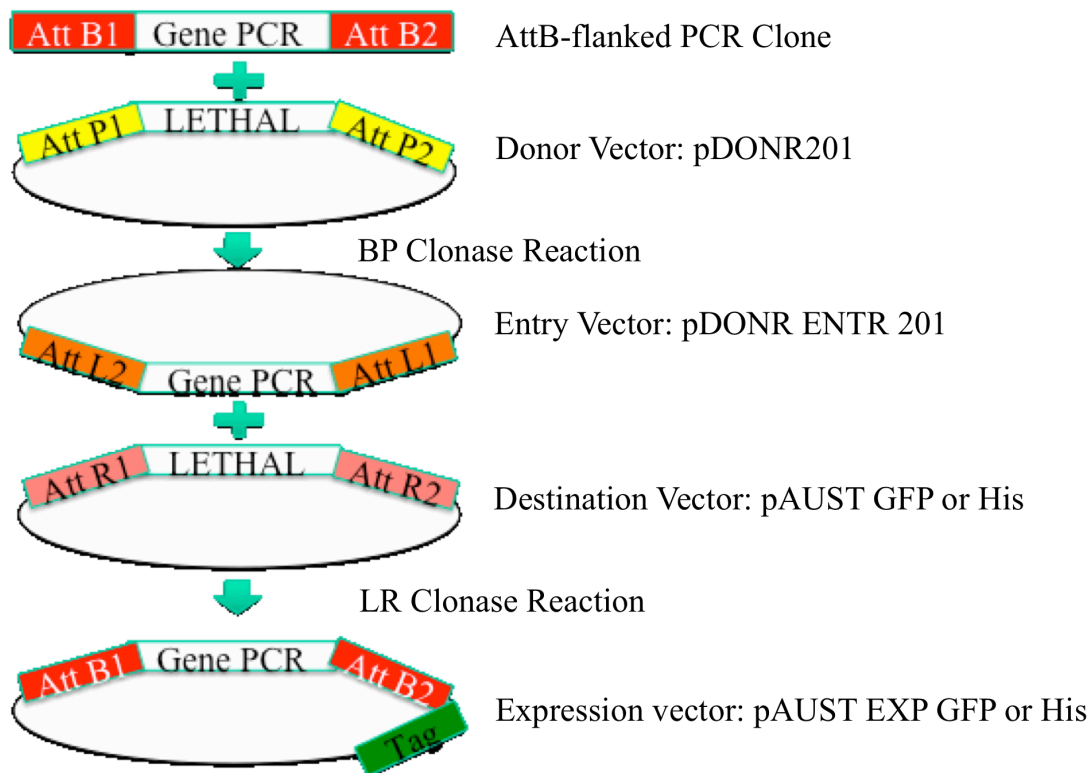


Figure 12 - Schematic of expression clone generation

Through a series of cloning steps, an expression vector can be generated with a C-terminal fusion tag which can be detected by immunoblotting. Because each starting vector contains a lethal gene (*ccdB*), only cells transformed with recombinant plasmids survive.

PCR-based Generation of AttB Flanked Genes

The AttB-flanked genes were generated by PCR for 4 of the genes of interest: *abi-1*, *lin-53*, *mig-10b*, and *mig-10 RAPH* (See Methods). The original *mig-10* constructs used as

templates for the PCR were in pDEST32 from Invitrogen, a bait expression vector for the yeast two hybrid system. The original *lin-53*, *arx-3*, and *abi-1* constructs were in pPC86 vectors, a prey expression vector for the yeast two hybrid system. These original constructs were transformed into competent *E.coli*, and DNA was isolated using a miniprep. Due to time constraints, the *arx-3*, *mig-10a*, and *mig-10c* constructs weren't able to be amplified from the constructs that were available.

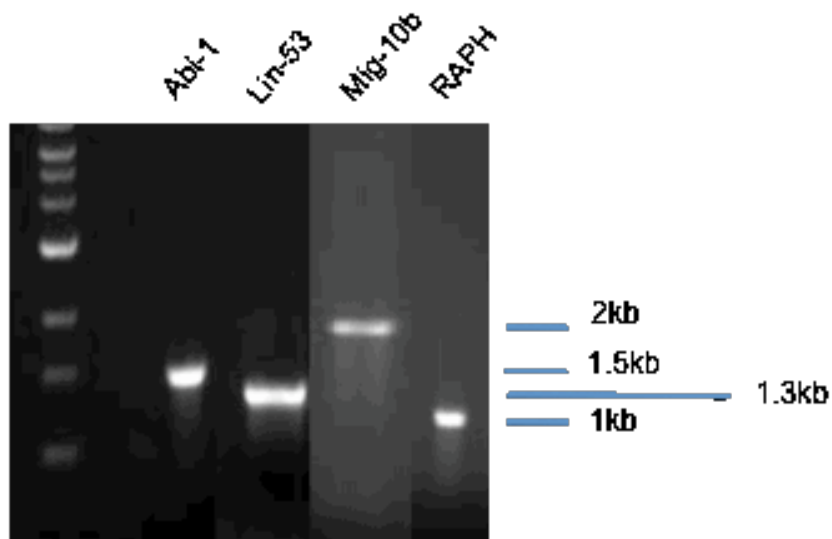


Figure 13 - Gel Analysis of PCR Clones

Analysis by gel electrophoresis showed that the PCR constructs generated were approximately the same size as calculated based on the sizes of the genes of interest (Figure 13).

Generation of Entry Vectors

In order to create an entry vector for each gene, the BP recombination reaction was performed on each PCR product generated. The recombination event to generate the entry vector was between the AttB-flanked PCR product, and pDONR201 AttP-flanked *ccdB* gene

(which is lethal in living cells) (Figure 14). The resulting entry vector contains an AttL flanked gene of interest (Figure 15). The AttL site is generated by recombination of the AttB and AttP sites. Following the BP reaction, DNA was transformed into cells, and individual colonies were selected, grown up, and isolated by miniprep. Correct integration of *mig-10b*, *mig-10 RAPH*, *abi-1*, and *lin-53* into the entry vector was confirmed by sequence analysis (data not shown).

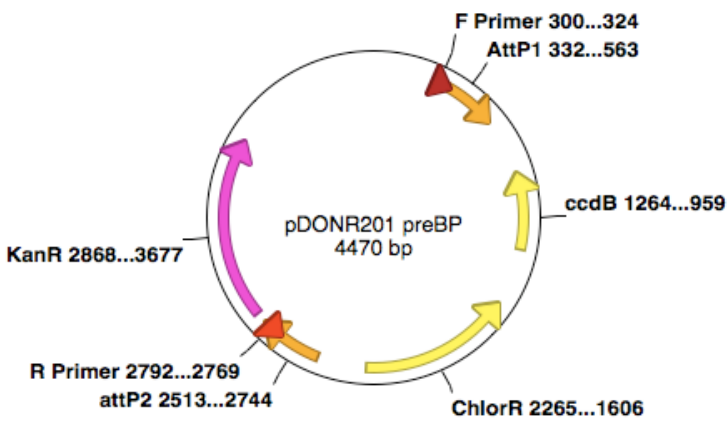


Figure 14 - pDONR201 vector map

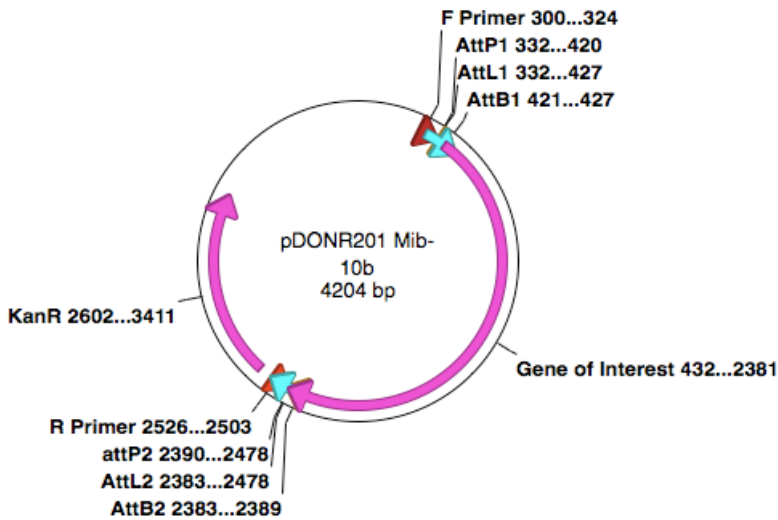


Figure 15 - Entry vector generated by recombination event with PCR product

Discussion

The study of neuronal development and repair in humans is extensive, involving investigations of the mechanisms by which neurons undergo growth and directed migration. MIG-10 has been characterized as a protein involved in the axonal growth and guidance of neurons in *C. elegans*. Its exact role in the signal transduction pathway for neuronal growth and migration - specifically, its interactions with other proteins in the pathway, remains unclear.

Analysis of the ABI-1 mutant phenotype, through quantification of *abi-1(tm494)* and *abi-1(tm494);abi-1(RNAi)*, revealed that a weak *abi-1* mutant allele leads to a weak excretory canal truncation phenotype which is significant over wildtype worms (for or both *abi-1(tm494)* and *abi-1(tm494);abi-1(RNAi)*, $p < 0.0001$). This shows that ABI-1 has function in the outgrowth of the excretory canal, and that the excretory canal truncation phenotype is an appropriate marker to look at the additive effects of ABI-1 mutants with other mutants.

Given the strong physical interaction between ABI-1 and MIG-10 seen through yeast two hybrid experiments, ABI-1 was suspected to interact with MIG-10 in the same pathway. It was expected that if the observed physical interaction was relevant *in vivo*, then *mig-10* mutant worms with knocked down expression of ABI-1 would not show significant changes in excretory canal outgrowth over *mig-10* mutants alone. The increased severity of the excretory canal phenotype of *mig-10(ct41)* mutants when fed on *abi-1(RNAi)*, however, suggests a genetic interaction: that these proteins function in different pathways that both lead to outgrowth of the excretory canal.

There are several possible explanations for the contradiction between the physical interaction seen in the yeast two hybrid screen, and the genetic interaction seen in the RNAi experiments. The first possible explanation is that the full effect of *abi-1(RNAi)* was not seen during the experimentation. With all that is known about ABI-1 *in vivo*, it is likely that a strong knockdown would be embryonic lethal. It is possible, therefore, that we are not seeing the full ABI-1 mutation phenotype in the excretory canal; an ABI-1 null mutant phenotype may be as severe as the phenotype seen in *mig-10(ct41);abi-1(RNAi)*, which would mean no increased severity in the phenotype was seen. Further testing must be done in RNAi sensitized strains to determine if this is the case.

Another possible explanation is that the original yeast two hybrid data was faulty. Mig-10a, the isoform used as the bait in the original screen, showed some self-activation in the yeast system and all data had to be compared to a relatively high background signal. To confirm that the interaction was not an artifact of the system, a second interaction study is currently being done utilizing co-immunoprecipitation of both ABI-1 and MIG-10 in insect cells. Time constraints and cloning difficulties forced the CoIP experiments to be halted

after the generation of the entry vector; however, due to the conflict between the RNAi data and the yeast two hybrid data, confirming the interactions with MIG-10 is an important experiment. The next step is the generation of the expression vector through the clonase LR reaction; once this is done, the vector is ready to be transfected into insect cells, and the CoIP experiments can be completed.

A third potential explanation leads to a possible mechanism of action for excretory canal outgrowth. Previous data has suggested that MIG-10 functions cell non-autonomously in the excretory canal, and that wild type function is necessary in the cells surrounding the excretory canal and not within the excretory canal itself (Manser et al., 1997). ABI-1 and UNC-53, however, are both believed to function together cell-autonomously in excretory canal outgrowth (Schmidt et. al, 2009). Analysis of the vertebrate homologue to MIG-10, RIAM, suggests that MIG-10 might function in an “inside out” pathway to promote expression of a cell-surface molecule involved in cell adhesion (Lafuente et al, 2004). This leads to a possible mechanism of action where ABI-1 and UNC-53 both function within the excretory cell to promote outgrowth of the excretory canal, and MIG-10 promotes surface expression of a receptor in underlying epidermal cells which provides a track for the excretory canal to grow along (Figure 17).

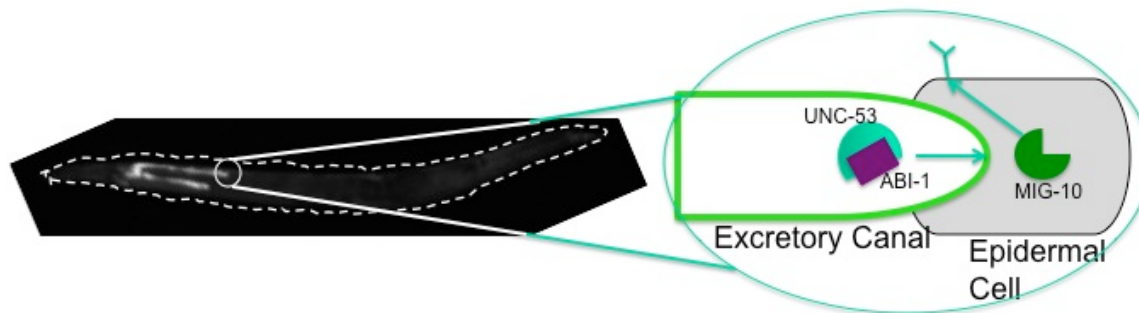


Figure 16 - MIG-10 does not function cell autonomously in excretory canal outgrowth

The genetic interaction seen between MIG-10 and ABI-1/UNC-53 suggests that MIG-10 functions in a separate pathway to promote excretory canal outgrowth. Previous data, which show that MIG-10 homologues promote cell adhesion, leads to a mechanism of action where MIG-10 is expressed in epidermal cells and promotes expression of receptor molecules that provide a track for the excretory canal to grow along. ABI-1 and UNC-53 function in the excretory canal to promote outgrowth.

There are, however, a few problems with this possible mechanism. If ABI-1 and UNC-53 function together in a pathway parallel to that of MIG-10, then an increase in the severity of the excretory canal phenotype should have been seen in the *mig-10(ct41);unc-53(RNAi)* mutant worms. There was a slight increase in severity, which bordered on statistically significant ($p=0.0504$), but not nearly as significant as *mig-10(ct41);abi-1(RNAi)* mutant worms ($p<0.0001$). In addition, there was no significant effect seen between *L440(RNAi)* worms and *unc-53(RNAi)* worms ($p=0.218$). It is therefore possible that had the RNAi been allowed to work for more generations or had been used in a sensitized strain, a statistically significant increase might have been seen.

A second problem with this proposed mechanism is that it does not take into account the strong physical interaction between MIG-10 and ABI-1 seen in the yeast two hybrid screen. However, since MIG-10 seems to function cell-autonomously in axon guidance, perhaps the physical interaction with ABI-1 is important in neurons rather than the excretory

cell, and mediates directed axon outgrowth. Further analysis of *abi-1(RNAi)*, both by itself and in a *mig-10(ct41)* background, needs to be done in strains which are susceptible to RNAi in the neurons. If a physical interaction occurs in the neurons, so that ABI-1 and MIG-10 are in the same pathway, then no increased severity of neuronal migration truncation should be seen between the double mutant (*mig-10(ct41);abi-1(RNAi)*) and each of the individual single mutants (*mig-10(ct41)* or *abi-1(RNAi)*).

The data generated from these experiments suggest that more research needs to be done to determine a full mechanism of action for the interaction between ABI-1 and MIG-10. Since both proteins are known to contribute to actin polymerization, their physical interaction would make sense; however, in this system, it is not possible to use the excretory canal as a model for neuronal migration. More research into the mechanism of excretory canal outgrowth, and other potential partners for both ABI-1 and MIG-10, might give a clearer picture about the cell non-autonomy of MIG-10. On the other hand, data studying the effect of knockdowns of both proteins in the neurons themselves would provide a clearer picture of neuronal migration, and potentially show whether or not the proteins do physically interact *in vivo*.

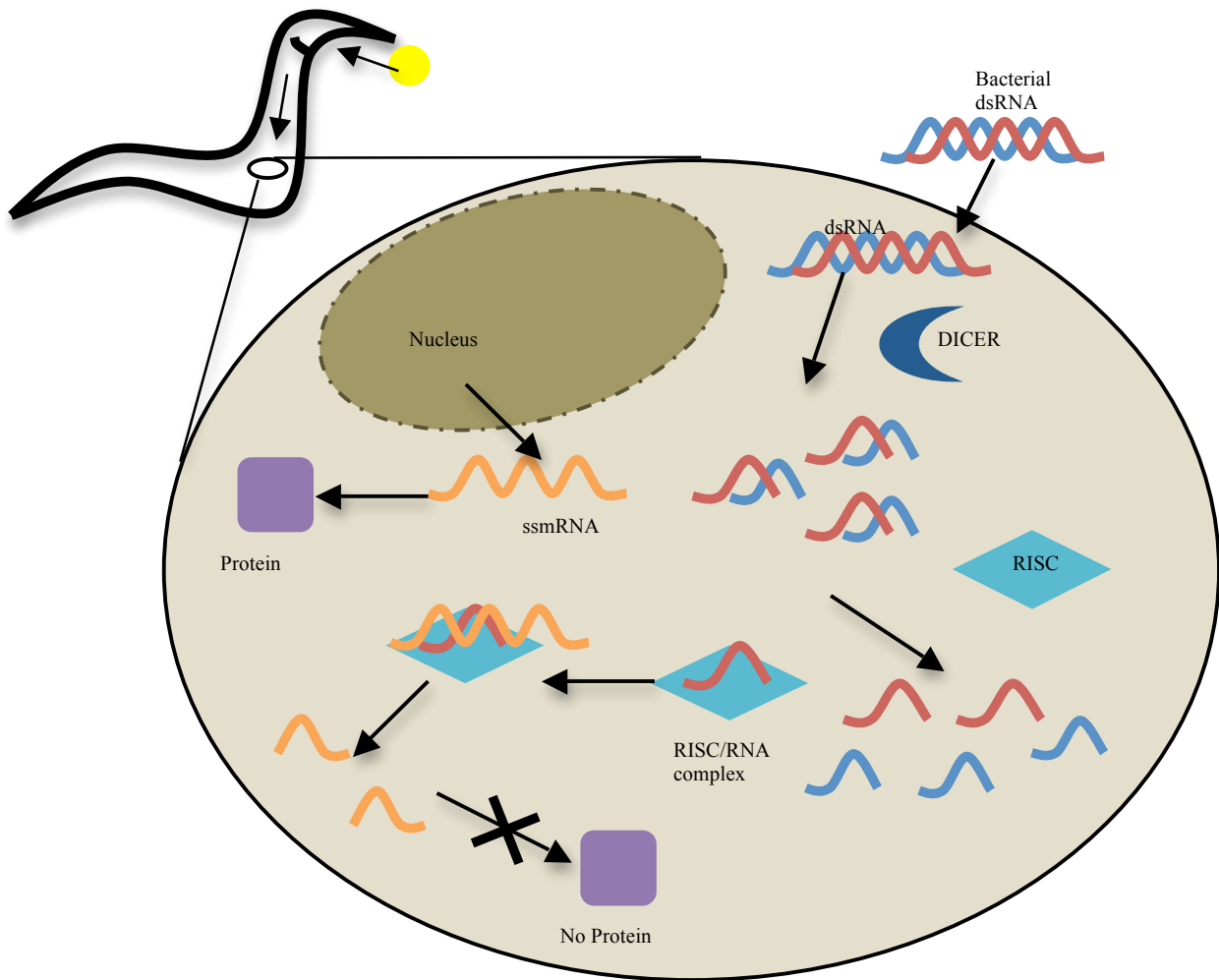
References

- Ahringer, Julie, 2003.** Clone Information and RNAi Feeding Protocol. Ahringer Lab.
- Bear M, Connors, Paradiso, 2001.** Neuroscience Exploring the Brain. 2nd edition:705-718.
- Chang C, Adler CE, Krause M, Clark SG, Gertler FB, Tessier-Lavigne M, Bargmann CI (2006).** MIG-10/Lamellipodin and AGE-1/PI3K Promote Axon Guidance and Outgrowth in Response to Slit and Netrin. *Current Biology* 16: 854-862.
- Echarri A, Lai MJ, Robinson MR, Pendergast AM, 2004.** Abl Interactor 1 (Abi-1) Wave-Binding and SNARE Domains Regulate Its Nucleocytoplasmic Shuttling, Lamellipodium Localization, and Wave-1 Levels. *Molecular and Cellular Biology* 24: 4979-4993.
- Fire A, Xu S, Montgomery MK, Kostas SA, Driver SE, Mello CC, 1998.** Potent and specific genetic interference by double-stranded RNA in *Caenorhabditis elegans*. *Nature* 391: 806-811.
- Gossellin, Jennifer and O'Toole, Sean, 2008.** Mig-10, an Adapter Protein, Interacts with ABI-1, a Component of Actin Polymerization Machinery. Major Qualifying Project.
- Hobert O, 2005.** Specification of the nervous system. *WormBook*, ed. The *C. elegans* Research Community, WormBook, doi/10.1895/wormbook.1.12.1, <http://www.wormbook.org>.
- Innocenti M, Zucconi A, Disanza A, Frittoli E, Areces LB, Steffen A, Stradal TEB, Di Fiore PP, Carlier MF, Scita G, 2004.** Abi1 is essential for the formation and activation of a WAVE2 signalling complex. *Nature Cell Biology* 6: 319-327
- Krause M, Leslie JD, Stewart M, Lafuente EM, Valderrama F, Jagannathan R, Strasser GA, Rubinson DA, Liu H, Way M, Yaffe MB, Boussiotis VA, Gertler FB, 2004.** Lamellipodin, an Ena/VASP Ligand, Is Implicated in the Regulation of Lamellipodial Dynamics. *Developmental Cell* 7: 571-583.
- Lafuente EM, van Puijenbroek AAFL, Krause M, Carman CV, Freeman GJ, Berezovskaya A, Constantine E, Springer TA, Gertler FB, Boussiotis VA, 2004.** RIAM, an Ena/VASP and Profilin Ligand, Interacts with Rap1-GTP and Mediates Rap-1 Induced Adhesion. *Developmental Cell* 7: 585-595.

- Manser J, Wood W, 1990.** Mutations Affecting Embryonic Cell Migrations in *Caenorhabditis elegans*. *Developmental Genetics* 11: 49-64.
- Manser J, Roonprapunt C, Margolis B, 1997.** *C. elegans* cell migration gene mig-10 shares similarities with a family of SH2 domain proteins and acts cell nonautonomously in excretory canal development. *Developmental Biology* 184: 150-164.
- Patel BN, Van Vactor DL, 2002.** Axon guidance: the cytoplasmic tail. *Current Opinion in Cell Biology* 14: 221-229.
- Phizicky EM, Fields S, 1995.** Protein-protein interactions: methods for detection and analysis. *Microbiology and Molecular Biology Reviews* 59: 99-100
- Proepper C, Johannsen S, Liebau S, Dahl J, Vaida B, Bockmann J, Kreutz MR, Gundelfinger ED, Boeckers TM, 2007.** Abelson interacting protein 1 (Abi-1) is essential for dendrite morphogenesis and synapse formation. *The EMBO Journal* 26: 1387-1409.
- Quinn CC, Pfeil DS, Wadsworth WG, 2008.** CED-10/Rac1 Mediates Axon Guidance by Regulating the Asymmetric Distribution of MIG-10/Lamellipodin. *Current Biology* 18: 1-6.
- Quinn CC, Pfeil DS, Chen E, Stovall EL, Harden MV, Gavin MK, Forrester WC, Ryder EF, Soto MC, Wadsworth WG, 2006.** UNC-6/Netrin and SLIT-1/Slit Guidance Cues Orient Axon Outgrowth Mediated by MIG-10/RIAM/Lamellipodin. *Current Biology* 16: 845-853.
- Schmidt KL, Marcus-Gueret N, Adeleye A, Webber J, Baillie D, Stringham EG, 2009.** The cell migration molecule UNC-53/NAV2 is linked to the ARP2/3 complex by ABI-1. *Development* 136: 563-574.
- Scita, G, Nordstrom J, Carbone R, Tenca P, Giardina G, Gutkind S, Bjarnegard M, Betsholtz C, Di Fiore PP, 1999.** EPS8 and E3B1 transduce signals from Ras to Rac. *Nature* 401: 290-293
- Yu TW, Bargmann CI, 2001.** Dynamic Regulation of Axon Guidance. *Nature Neuroscience* 4: 1169-1176.

Appendices

Appendix A: RNAi Method Diagram



Appendix B: Chi-Square Tests, Data Combination

Experiment	Plate	10	9	8	7	6	5	4	3	2	totals	x²
<i>mig-10(ct41);unc-22(RNAi)</i>	Primary	0	0	0	0	0	0	0	0	0	0	0
	Secondary	0									0	0
	Tertiary	2	0	12	17	10	0	0	0	0	41	0
Totals		2	0	12	17	10	0	0	0	0	41	0

#N/A

Experiment	Plate	10	9	8	7	6	5	4	3	2	totals	x²
<i>mig-10(ct41);abi-1(RNAi)</i>	Primary	20	2	16	3	7	0	0	0	0	48	2.0166
	Secondary	32	5	12	3	11	0	0	0	0	63	1.5365
	Tertiary	0	0	0	0	0	0	0	0	0	0	0
Totals		52	7	28	6	18	0	0	0	0	111	3.5531

accept H0
p=0.47

Experiment	Plate	10	9	8	7	6	5	4	3	2	totals	x²
<i>mig-10(ct41);unc-53(RNAi)</i>	Primary	0	4	9	4	4	0	0	0	0	21	2.1211
	Secondary	7	11	32	10	16	0	0	0	0	76	2.4001
	Tertiary	3	4	11	13	9	0	0	0	0	40	4.9408
Totals		10	19	52	27	29	0	0	0	0	137	9.462

accept H0
p=0.305

Experiment	Plate	10	9	8	7	6	5	4	3	2	totals	x²
<i>mig-10(ct41);L440(RNAi)</i>	Primary										0	0
	Secondary	3	5	22	24	23	0	0	0	0	77	1.8773
	Tertiary	8	6	26	18	28	0	0	0	0	86	1.6809
Totals		11	11	48	42	51	0	0	0	0	163	3.5582

accept H0
p=0.469

Experiment	Plate	10	9	8	7	6	5	4	3	2	totals	x²
<i>mig-10(RNAi)</i>	Primary	0	0	0	0	0	0	0	1	27	28	17.628
	Secondary	0	0	0	0	0	0	0	0	0	0	0
	Tertiary	0	0	0	1	3	6	6	6	4	26	18.984
Totals		0	0	0	1	3	6	6	7	31	54	36.612

reject H0
p=1e-6

Experiment	Plate	10	9	8	7	6	5	4	3	2	totals	x²
<i>abi-1(RNAi)</i>	Primary	0	0	0	0	1	2	8	15	31	57	3.9746
	Secondary	0	0	0	0	0	0	1	10	21	32	2.6008
	Tertiary	0	0	0	0	0	0	2	5	24	31	2.9713
Totals		0	0	0	0	1	2	11	30	76	120	9.5466

accept H0
p=0.298

Experiment	Plate	10	9	8	7	6	5	4	3	2	totals	x²
<i>unc-53(RNAi)</i>	Primary	0	0	0	0	0	2	6	7	13	28	4.0905
	Secondary	0	0	0	0	0	0	1	1	18	20	5.7267
	Tertiary	0	0	0	0	0	0	0	0	0	0	0
Totals		0	0	0	0	0	2	7	8	31	48	9.8172

reject H0
p=0.020

Experiment	Plate	10	9	8	7	6	5	4	3	2	totals	x²
<i>L440(RNAi)</i>	Primary										0	0
	Secondary										0	0
	Tertiary	0	0	0	0	0	1	8	25	45	79	0
Totals		0	0	0	0	0	1	8	25	45	79	0

#N/A

Experiment	Plate	10	9	8	7	6	5	4	3	2	totals	x²
<i>abi-1(tm494);abi-1(RNAi)</i>	Primary										0	0
	Secondary	0	0	0	1	2	2	8	2	0	15	1.2655
	Tertiary	0	0	0	0	0	0	3	3	0	6	3.1636
Totals		0	0	0	1	2	2	11	5	0	21	4.4291

accept H0
p=0.351

Experiment	Plate	10	9	8	7	6	5	4	3	2	totals	x²
<i>abi-1(tm494)</i>											0	0
	Parental	0	0	0	0	1	0	24	15	3	43	5.5933
	F1	0	0	0	0	1	2	9	19	10	41	9.8766
	F2	0	0	0	0	0	0	17	20	4	41	2.075
Totals		0	0	0	0	2	2	50	54	17	125	17.545

reject H0
p=0.025

Experiment	Plate	10	9	8	7	6	5	4	3	2	totals	x²
<i>mig-10(ct41)</i>	20 C										0	0
	Parental	1	0	15	14	13	0	0	0	0	43	2.7295
	F1	1	2	14	8	18	0	0	0	0	43	5.1433
	F2	0	4	18	13	3	0	0	0	0	38	9.8169
Totals		2	6	47	35	34	0	0	0	0	124	17.69

reject H0
p=0.024

Experiment	Plate	10	9	8	7	6	5	4	3	2	totals	x²
<i>Wildtype</i>	20 C										0	0
	Parental	0	0	0	0	0	0	1	0	39	40	0.1766
	F1	0	0	0	0	0	0	0	0	40	40	0.6723
	F2	0	0	0	0	0	0	1	0	40	41	0.1559
Totals		0	0	0	0	0	0	2	0	119	121	1.0047

accept H0
p=0.605

Appendix C: Chi-Square Test, Strain Comparisons

Comparison	10	9	8	7	6	5	4	3	2	Totals	X2
<i>abi-1(RNAi)</i>	0	0	0	0	1	2	11	30	76	120	0.7282055
<i>L440(RNAi)</i>	0	0	0	0	0	1	8	25	45	79	1.106134937
Totals	0	0	0	0	1	3	19	55	121	199	1.834340437

accept H0
p=0.766

Comparison	10	9	8	7	6	5	4	3	2	Totals	X2
<i>mig-10(ct41);abi-1(RNAi)</i>	52	7	28	6	18	0	0	0	0	111	40.57457539
<i>mig-10(ct41);L440(RNAi)</i>	11	11	48	42	51	0	0	0	0	163	27.63053907
Totals	63	18	76	48	69	0	0	0	0	274	68.20511446

reject H0
p<0.0001

Comparison	10	9	8	7	6	5	4	3	2	Totals	X2
<i>mig-10(ct41);abi-1(RNAi)</i>	52	7	28	6	18	0	0	0	0	111	118.0284495
<i>abi-1(RNAi)</i>	0	0	0	0	1	2	11	30	76	120	109.1763158
Totals	52	7	28	6	19	2	11	30	76	231	227.2047653

reject H0
p<0.0001

Comparison	10	9	8	7	6	5	4	3	2	Totals	X2
<i>unc-53(RNAi)</i>	0	0	0	0	0	2	7	8	31	48	2.758012693
<i>L440(RNAi)</i>	0	0	0	0	0	1	8	25	45	79	1.675754547
Totals	0	0	0	0	0	3	15	33	76	127	4.43376724

accept H0
p=0.218

Comparison	10	9	8	7	6	5	4	3	2	Totals	X2
<i>mig-10(ct41);unc-53(RNAi)</i>	10	19	52	27	29	0	0	0	0	137	5.145158
<i>mig-10(ct41);L440(RNAi)</i>	11	11	48	42	51	0	0	0	0	163	4.324457951
Totals	21	30	100	69	80	0	0	0	0	300	9.46961595

accept H0
p=0.0504

Comparison	10	9	8	7	6	5	4	3	2	Totals	X2
<i>mig-10(ct41);unc-53(RNAi)</i>	10	19	52	27	29	0	0	0	0	137	48
<i>unc-53(RNAi)</i>	0	0	0	0	0	2	7	8	31	48	137
Totals	10	19	52	27	29	2	7	8	31	185	185

reject H0
p<0.0001

Comparison	10	9	8	7	6	5	4	3	2	Totals	X2
<i>mig-10(ct41);unc-22(RNAi)</i>	2	0	12	17	10	0	0	0	0	41	5.001212136
<i>mig-10(ct41);L440(RNAi)</i>	11	11	48	42	51	0	0	0	0	163	1.257973605
Totals	13	11	60	59	61	0	0	0	0	204	6.25918574

accept H0
p=0.181

Comparison	10	9	8	7	6	5	4	3	2	Totals	X2
<i>mig-10(ct41);L440(RNAi)</i>	11	11	48	42	51	0	0	0	0	163	2.838569032
<i>mig-10(ct41)</i>	2	6	47	35	34	0	0	0	0	124	3.731344776
Totals	13	17	95	77	85	0	0	0	0	287	6.569913809

accept H0
p=0.16

Comparison	10	9	8	7	6	5	4	3	2	Totals	X2
<i>L440(RNAi)</i>	0	0	0	0	0	1	8	25	45	79	34.2849645
<i>Wild Type</i>	0	0	0	0	0	0	2	0	119	121	22.38439831
Totals	0	0	0	0	0	1	10	25	164	200	56.6693628

reject H0
p<0.0001

Comparison	10	9	8	7	6	5	4	3	2	Totals	X2
<i>abi-1(tm494);abi-1(RNAi)</i>	0	0	0	1	2	2	11	5	0	21	16.59385544
<i>abi-1(tm494)</i>	0	0	0	0	2	2	50	54	17	125	2.787767713
Totals	0	0	0	1	4	4	61	59	17	146	19.38162315

reject H0

p=0.0016